The interaction of electrons with optical phonons in embedded circular and elliptical GaAs quantum wires



1995 J. Phys.: Condens. Matter 7 9819

(http://iopscience.iop.org/0953-8984/7/50/016)

J. Phys.: Condens. Matter 7 (1995) 9819–9831. Printed in the UK

# The interaction of electrons with optical phonons in embedded circular and elliptical GaAs quantum wires

C R Bennett, N C Constantinou, M Babiker and B K Ridley
Department of Physics, University of Essex, Colchester CO4 3SQ, UK

Received 12 May 1995

**Abstract.** We consider electronic intrasubband transitions involving the confined and interface optical phonons of circular and elliptical GaAs quantum wires. Detailed treatments are given for a GaAs wire embedded in AlAs where the electrons are confined via an infinite potential barrier. The optical phonons are described using the dielectric continuum (DC) model, which for the GaAs/AlAs system compares favourably with more sophisticated macroscopic models and *ab initio* microscopic calculations in its prediction for the *total* scattering rates. The DC model has been applied previously to the circular case, but here we evaluate the rates analytically. It is shown that the behaviour of the electrons and phonons in elliptical wires is both quantitatively and qualitatively different from that in circular wires, especially as regards angular properties.

## 1. Introduction

The interaction of electrons with the polar optical modes is of prime importance both in bulk materials and in low-dimensional semiconductor systems. Whilst the boundary conditions on the electronic wavefunctions are well established for the GaAs/AlAs system [1], those appropriate for the optical phonons have been the subject of much discussion over the past few years. Continuum models which incorporate both electrostatic and mechanical boundary conditions [2] and microscopic lattice dynamic models [3, 4] both predict that the *total* electron–optical phonon scattering rates are close to those evaluated by the dielectric continuum (DC) model (see, e.g. [5, 6]) in the GaAs/AlAs and GaAs/AlGaAs systems, although the spectrum for the phonon modes is in reality more complicated than those of the DC model. Since our main concern in this paper is with the GaAs/AlAs system we take advantage of the relative simplicity of this model and employ it in the calculation of total scattering rates. The phonon spectrum in the DC model consists of an infinite set of confined modes which have vanishing electrostatic potentials at the interfaces and oscillate at the bulk LO frequency of GaAs, together with a set of modes which have potential maxima at the interfaces (the interface modes). These interface modes have frequencies within the *reststrahl* bands of GaAs and AlAs and, in the quasi-two-dimensional (Q2D) systems, it is found both theoretically [3, 6, 7] and experimentally [8, 9] that the AlAs interface modes dominate the interaction under certain circumstances.

In this paper we report results of the interaction of electrons with the DC phonons of a GaAs wire of elliptical cross-section (henceforth elliptical wire) embedded in AlAs. Investigations of the scattering rates for embedded wires using bulk phonons [10–14], the DC model [15–18], and the hydrodynamic (HD) model [19] have already been reported, although the latter model is now regarded as inappropriate for the evaluation of scattering

0953-8984/95/509819+13$19.50  

rates in the GaAs/AlAs system [2–4]. In [19], however, the HD model was applied to the free-standing system and in this system the potentials derived by the HD model are just those of the DC model. Microscopic calculations appropriate for rectangular wires have also been reported recently [20].

The plan of this paper is as follows. Section 2 describes the confined and interface modes of a GaAs wire or circular cross-section (henceforth circular wire) and intrasubband scattering rates are obtained in analytical form for the first time. Section 3 describes the electronic states of an elliptical wire and section 4 the confined and interface modes of an elliptical wire. In section 5 numerical results of the intrasubband scattering rates are presented in detail for the elliptical wire and a comparison is made with the results of the circular wire. Section 6 contains our conclusions.

In what follows all the relevant material parameters used are those tabulated in the review article by Adachi [21].

## 2. Analytical scattering rates for a circular wire

We consider a GaAs (material 1) circular wire of radius $R$ embedded in AlAs (material 2). The confined modes within the wire have vanishing Coulomb potentials at the boundary and oscillate at the zone-centre LO-phonon frequency of GaAs. The quantized potential operator for the confined modes is

$$\hat{\Phi}(\boldsymbol{R}) = \sum_{q}\sum_{mn}\left\{\Phi_{mnq}(\boldsymbol{R})a_{mn}(q) + \Phi^{*}_{mnq}(\boldsymbol{R})a^{\dagger}_{mn}(q)\right\} \tag{1}$$

where $a_{mn}(q)$ are Boson operators.

$$\Phi_{mnq}(\boldsymbol{R}) = A_{mn}J_m\left(\tilde{q}_{mn}r\right)\mathrm{e}^{\mathrm{i}qz}\,\mathrm{e}^{\mathrm{i}m\phi} \qquad m = 0, \pm 1, \pm 2, \ldots. \tag{2}$$

In the above $A_{mn}$ is the normalization factor, $q$ the axial wavevector and $\tilde{q}_{mn}$ is the confinement wavevector which is related to $\alpha_{mn}$, the $n$th zero of the Bessel function $J(x)$, via $\tilde{q}_{mn} = \alpha_{mn}/R$. The explicit form of the normalization factor is

$$A_{mn} = \sqrt{\left[\hbar\omega_{L1}/\left[2\varepsilon_0 V J^2_{m+1}\left(\alpha_{mn}\right)\left(q^2 + \tilde{q}^2_{mn}\right)\right]\right]\left(1/\varepsilon_{\infty 1} - 1/\varepsilon_{s1}\right)} \tag{3}$$

where $\varepsilon_{\infty 1\,(s1)}$ is the high- (low-) frequency dielectric constant for GaAs and $V$ is the volume of the wire. The DC confined modes of a cylinder are now quantized and our expressions for the corresponding potentials agree with those of [15].

We now turn to the description of the interface modes of the circular wire. The dispersion relation has been known for a long time (see e.g. [22]) and has been recently observed [23]. The dispersion relation is derived as follows. The potential for the interface modes is written as

$$\Phi_{mq}(\boldsymbol{R}) = \begin{cases} B_{mq}I_m(qr)\mathrm{e}^{\mathrm{i}qz}\,\mathrm{e}^{\mathrm{i}m\phi} & r \leqslant R \\ C_{mq}K_m(qr)\mathrm{e}^{\mathrm{i}qz}\,\mathrm{e}^{\mathrm{i}m\phi} & r > R \end{cases} \tag{4}$$

where $I_m(x)$ and $K_m(x)$ are modified Bessel functions. The amplitudes $C_{mq}$ and $B_{mq}$ are obtained from the normalization condition together with the dispersion relations. The dispersion relation for the interface modes of the cylinder is obtained from the electrostatic boundary conditions at $r = R$ (namely continuity of $\Phi$ and $\varepsilon\,\partial\Phi/\partial r$) and is given by

$$\varepsilon_1\left(\omega_{mq}\right)/\varepsilon_2\left(\omega_{mq}\right) = I_m(qR)K'_m(qR)/I'_m(qR)K_m(qR) \tag{5}$$

where the primes indicate differentiation with respect to the argument of the Bessel functions. We follow the procedure of Knipp and Reinecke [24] and display the interface mode

dispersion by plotting the quantity $P$ which is independent of the material parameters and is given by

$$P = [\varepsilon_1(\omega_{mq}) + \varepsilon_2(\omega_{mq})]/[\varepsilon_1(\omega_{mq}) - \varepsilon_2(\omega_{mq})] \qquad -1 \leqslant P \leqslant 1. \quad (6)$$

From equation (6) it is seen that $P$ is unity when $\omega_{mq}$ corresponds to the zone-centre GaAs TO- and AlAs LO-phonon frequency, and $P = -1$ when $\omega_{mq}$ corresponds to the zone-centre GaAs LO- and AlAs TO-phonon frequency. In other words $P$ spans the *reststrahl* bands of the two materials. The vanishing of $P$ corresponds to the frequency of the two surface modes on a planar GaAs/AlAs interface or the single GaAs/vacuum surface mode for the free-standing wire. The density of interface modes is highest near $P = 0$. The variation of $P$ with the axial wavevector is depicted in figure 1.

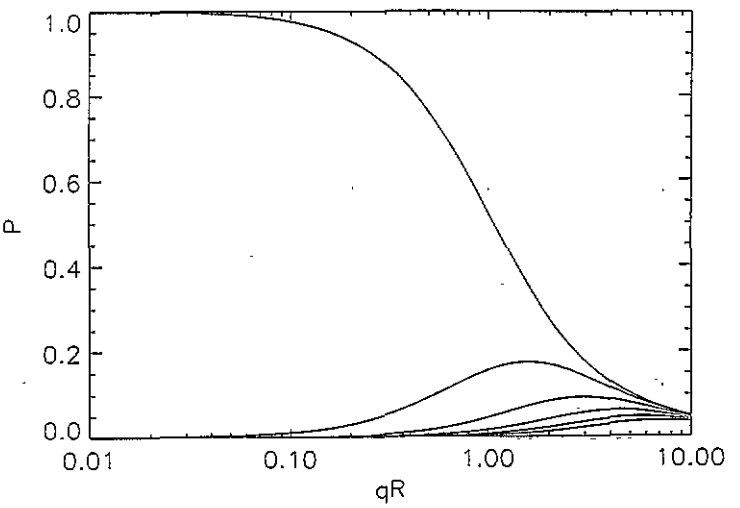


**Figure 1.** $P$ as a function of $qR$ (equation (6)) for a circular wire (from top to bottom we have $|m| = 0, 1, 2, 3, 4, 5$).

It is straightforward to quantize the potential associated with the interface modes and we find

$$B_{mq} = \sqrt{\hbar\varepsilon_2(\omega_{mq})R/q\varepsilon_0 V I_m(qR)I'_m(qR)D(\omega_{mq})}$$
$$C_{mq} = [I_m(qR)/K_m(qR)]B_{mq}. \quad (7)$$

It should be noted that only the results for $m = 0$ are quoted in [15] and these are in agreement with the above results. In (7) the factor $D(\omega_{mq})$ is given by

$$D(\omega_{mq}) = (\varepsilon_2(\omega)\partial\varepsilon_1(\omega)/\partial\omega - \varepsilon_1(\omega)\partial\varepsilon_2(\omega)/\partial\omega)_{\omega=\omega_{mq}}. \quad (8)$$

The quantized potential operator for the interface modes has now been determined. We are now in a position to evaluate the electronic intrasubband rates.

The effective mass Schrödinger equation for an electron confined via hard walls to a circular wire is exactly solvable in terms of Bessel functions [10]. Unfortunately, these do not yield analytical results for the form factors. Since we are only interested in intrasubband scattering within the lowest subband, we may employ the approximate ground state wavefunction proposed by Gold and Ghazali [25]

$$\Psi_{0k}(R) = \sqrt{3/V}(1 - r^2/R^2)e^{ikz} \qquad E_0 = 6\hbar^2/2m^*R^2. \quad (9)$$

The above approximation wavefunction has been recently employed to calculate analytical rates for scattering with bulk phonons by Masale and Constantinou [26] and properties of plasmons in cylindrical wires by Wendler and Grigoryan [27].

The intrasubband scattering rate, $W$, for scattering within the first subband via emission of confined modes is obtained via Fermi's golden rule and we find

$$W = W_0 \frac{[N(\omega_{L1}+1]}{\sqrt{\tilde{E}_k - 1}} \sum_{n=1}^{\infty} \frac{\Xi_n^2}{J_1^2(\alpha_{0n})} \left[ \frac{1}{Q_+^2 + \alpha_{0n}^2} + \frac{1}{Q_-^2 + \alpha_{0n}^2} \right] \tag{10}$$

where $\tilde{E}_k = E_k/\hbar\omega_{L1}$. The quantities $Q_\pm$ and $\Xi_n$ are given by

$$Q_\pm = \left(2m^*\omega_{L1}/\hbar\right)^{1/2} R_p \left[\sqrt{\tilde{E}_k} \pm \sqrt{\tilde{E}_k - 1}\right] \tag{11}$$

$$\Xi_n = \left(48/\alpha_{0n}^3\right) J_3(\alpha_{0n}). \tag{12}$$

The quantity $W_0$ is defined by

$$W_0 = \left(e^2/4\pi\varepsilon_0\hbar\right)\left(2m^*\omega_{L1}/\hbar\right)^{1/2}\left(1/\varepsilon_{\infty 1} - 1/\varepsilon_{s1}\right) \tag{13}$$

and for GaAs $W_0$ is approximately $8.7 \times 10^{12}$ s$^{-1}$. The scattering rate given by equation (10) is essentially that obtained by Constantinou and Ridley [19], the only difference being that the modes were dispersive in [19].

The intrasubband scattering rate for coupling to the cylindrical interface modes is given by

$$W = 2W_0 \left( \frac{1}{\varepsilon_{\infty 1}} - \frac{1}{\varepsilon_{s1}} \right)^{-1} \sum_{q_0} \left| \frac{\omega_{L1}\varepsilon_2}{D(\omega_{0q_0})} \right| \frac{[N(\omega_{0q_0})+1]\Xi_{q_0}^2}{G(\tilde{E}_k)|q_0 R| I_0(q_0 R) I_1(q_0 R)} \tag{14}$$

where $q_0$ is a zero of

$$q^2 - 2kq + 2m^*\omega_{mq}/\hbar = 0 \tag{15}$$

and

$$G(\tilde{E}_k) = \left| \sqrt{\tilde{E}_k} - \sqrt{\hbar q_0^2/2m^*\omega_{L1}} - \sqrt{m^* v_g^2/2\hbar\omega_{L1}} \right| \tag{16}$$

with $v_g (= \partial\omega_{mq_0}/\partial q)$ the group velocity of the interface mode at $q = q_0$. In equation (14) $\Xi_q$ is the analogue of (12) for the interface modes and is given by

$$\Xi_q = (48/(qR)^3) I_3(qR) \tag{17}$$

and we note that $\Xi_q \to 1$ as $qR \to 0$.

The scattering rate for a GaAs quantum wire of radius 70.7 Å embedded in AlAs is displayed in figure 2 as a function of the axial energy. The discontinuities in the rates arise from the singularity in the one-dimensional density of states, and this type of behaviour by the scattering rate in quasi-one-dimensional systems is well known. The discontinuities may, if necessary, be smoothed out phenomenologically by an *ad hoc* broadening of the density of states [28] which will arise in practice due to various mechanisms such as the fluctuations in the wire boundary. It should be noted that the contribution of the GaAs interface modes in this system is marginal. The main contribution originates from the confined GaAs modes, and, for energies above approximately 48 meV, the AlAs interface mode as well. Also plotted in figure 2 are the rates using bulk three-dimensional GaAs and AlAs phonons (in calculating the scattering rate via bulk AlAs LO modes we take the GaAs effective mass, all other parameters being the AlAs ones). Note that this often-made assumption of bulk phonons does not completely reproduce the complex behavior of the scattering rates, although away from the singularities the assumption of bulk GaAs phonons is not too bad an approximation to the overall rate.

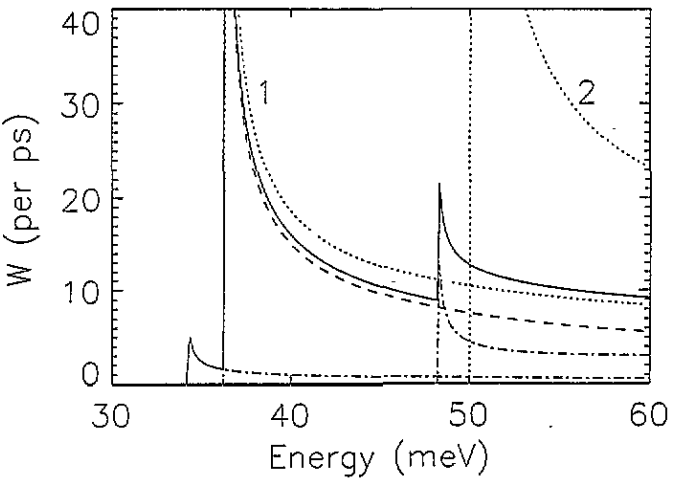


**Figure 2.** The scattering rate as a function of axial energy for an $R = 70.7$ Å GaAs circular wire embedded in AlAs. The solid curve represents the total scattering rate from all the allowed modes. The dashed curve is the contribution from the GaAs ($m = 0$) confined modes; the dot–dashed curve which makes the smallest contribution represents the rate from the $m = 0$ GaAs interface mode and the other dot–dashed curve which makes a more significant contribution is that due to the $m = 0$ AlAs interface mode. The dashed curve labelled 1 is the scattering rate assuming bulk GaAs phonons whilst that labelled 2 is the rate assuming AlAs bulk phonons.

## 3. The electronic states of an elliptical quantum wire

We consider an elliptical GaAs wire with semimajor axis $a$ and semiminor axis $b$. We assume that the electrons are confined in GaAs by an infinite barrier. In elliptical co-ordinates $\boldsymbol{R} = (u, v, z)$ with $u$ the 'radial' co-ordinate, $v$ the 'angular' co-ordinate and $z$ the axial co-ordinate, Schrödinger's equation (as is Laplace's) is separable with the wavefunction given by

$$\Psi(\boldsymbol{R}) = A\,\mathrm{e}^{\mathrm{i}kz}\,U(u)V(v) \tag{18}$$

where $k$ is the axial wavevector. The radial ($U$) and angular ($V$) components of the wavefunction satisfy the equations

$$\mathrm{d}^2U(u)/\mathrm{d}u^2 - (\beta - 2\lambda\cosh(2u))U(u) = 0 \tag{19}$$

$$\mathrm{d}^2V(v)/\mathrm{d}v^2 + (\beta - 2\lambda\cos(2v))V(v) = 0 \tag{20}$$

which are the equations of Mathieu [29]. The angular functions are periodic ($V(v+2\pi) = V(v)$) which implies that the separation constants $\beta$ (denoted $\beta_m$) are quantized and labelled by the azimuthal quantum number $m$. The solutions to the above equations which are regular at the origin are

$$\Psi_{mnk}(\boldsymbol{R}) = A_{mn}\,\mathrm{e}^{\mathrm{i}kz}\begin{cases}\mathrm{Ce}_m(u,\lambda_{mn})\mathrm{ce}_m(v,\lambda_{mn}) & \text{even}\\ \mathrm{Se}_m(u,\lambda_{mn})\mathrm{se}_m(v,\lambda_{mn}) & \text{odd}\end{cases} \tag{21}$$

and our notation for all of the Mathieu functions employed in this work is standard [29]. In (21) $\lambda_{mn}$ is given by

$$\lambda_{mn} = \tfrac{1}{4}f^2\tilde{k}_{mn}^2 \tag{22}$$

with $f$ the semifocal distance ($= ae$ with $e$ the eccentricity); $\tilde{k}_{mn}$ is the confinement wavevector of the electron in the $x$–$y$ plane. The labels odd and even refer to the parity of the angular functions with respect to $v$. The Mathieu functions with index $m$ even have periodicity $\pi$ whilst those with $m$ odd have periodicity $2\pi$. The requirement that the above wavefunction vanishes at $u_0$ which is given by

$$u_0 = \cosh^{-1}(1/e) \tag{23}$$

yields the quantum number $n$. The $n$th root of the radial component is labelled $\lambda_{mn}$. The normalization factor $A_{mn}$ is given by

$$A_{mn}^{-2} = L_z \int_0^{2\pi} \int_0^{u_0} U_m^2(u, \lambda_{mn}) V_m^2(u, \lambda_{mn}) f^2(\sinh^2(u) + \sin^2(v)) \, du \, dv \tag{24}$$

where $L_z$ is the length of the elliptical wire which, as for the circular wire, is assumed to be effectively infinite. The total energy of the state $(m, n, k)$ is given by

$$E_{mnk} = (\hbar^2/2m^*)\left[\tilde{k}_{mn}^2 + k^2\right]. \tag{25}$$

Figure 3 illustrates the confinement energy as a function of $a/b$ for fixed $b = 50$ Å. It is noted that both the cylindrical ($e = 0$) and the slab ($e \to 1$) limits are obtainable, with the degeneracy in the cylindrical states lifted by the elliptical asymmetry. The number of electronic states within the energy interval shown in figure 3 increases dramatically as $e$ approaches unity, and we only show a few of the states in this regime.

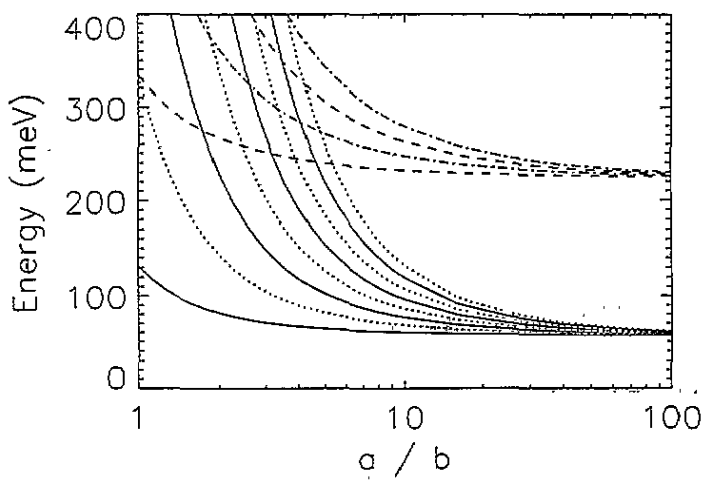


**Figure 3.** The subband energies of an elliptical wire with $b = 50$ Å as a function of $a/b$. The solid curves correspond to even states with period $\pi$, the dotted curves are even states with period $2\pi$, the dashed curves are odd states with period $\pi$ and the dashed–dot curves are odd states with period $2\pi$.

We pause here to mention that as the eccentricity increases the ground state wavefunction tends to be localized near the region of lowest curvature, in other words towards the centre of the ellipse. This, as we demonstrate in the following section, is in contrast to the behaviour of the elliptical interface mode. A more detailed explanation of this behaviour is given elsewhere [30].

Our next task is to consider the optical phonons. Fortunately, as demonstrated below, the above formalism for the electrons also describes the form of the potentials for the various optical modes via a redefinition of $\lambda$.

## 4. The confined and interface optical phonons of an elliptical quantum wire

The potential associated with the confined modes can be shown, by direct analogy with the electron calculation outlined above, to have the form (we follow closely the derivation of [24])

$$\Phi_{mnq}(R) = B_{mn}\,\mathrm{e}^{\mathrm{i}qz}\begin{cases}\mathrm{Ce}_m(u,\lambda_{mn})\mathrm{ce}_m(v,\lambda_{mn}) & \text{even}\\ \mathrm{Se}_m(u,\lambda_{mn})\mathrm{se}_m(v,\lambda_{mn}) & \text{odd}\end{cases} \tag{26}$$

with $q$ the phonon axial wavevector; $B_{mn}$ are normalization constants and

$$\lambda_{mn} = \tfrac{1}{4}f^2\tilde{q}_{mn}^2 \tag{27}$$

with $\tilde{q}_{mn}$ the phonon confinement wavevector in the $x$–$y$ plane. Because of the boundary conditions, the potentials for the *confined* modes are completely analogous to the electron wavefunctions and have exactly the same form.

The potentials associated with the interface modes satisfy equations (19) and (20) with

$$\lambda = -\tfrac{1}{4}f^2q^2 \tag{28}$$

and have the form

$$\Phi_{mq}(R) = C_m\,\mathrm{e}^{\mathrm{i}qz}\,U_m(u)V_m(v) \tag{29}$$

where $C_m$ is the normalization constant, and the radial and angular functions are given by

$$U_m(u) = \begin{cases}\mathrm{Ce}_m(u,\lambda_m)\mathrm{Fek}_m(u_0,\lambda_m) & u \leqslant u_0\\ \mathrm{Fek}_m(u,\lambda_m)\mathrm{Ce}_m(u_0,\lambda_m) & u > u_0\end{cases} \qquad V_m(v) = \mathrm{ce}_m(v,\lambda_m)\ \text{even} \tag{30}$$

$$U_m(u) = \begin{cases}\mathrm{Se}_m(u,\lambda_m)\mathrm{Gek}_m(u_0,\lambda_m) & u \leqslant u_0\\ \mathrm{Gek}_m(u,\lambda_m)\mathrm{Se}_m(u_0,\lambda_m) & u > u_0\end{cases} \qquad V_m(v) = \mathrm{se}_m(v,\lambda_m)\ \text{odd}. \tag{31}$$

In equations (30) and (31) the relevant Mathieu functions are those which are finite at the origin and vanish at infinity.

The dispersion relation for the interface modes is obtained from the usual electrostatic boundary conditions and may be expressed in the following way:

$$\frac{\varepsilon_1(\omega_{mq})}{\varepsilon_2(\omega_{mq})} = \frac{\left((\partial/\partial u)\,\ln\left[\mathrm{Fek}_m(u,\lambda_m)\right]\right)_{u=u_0}}{\left((\partial/\partial u)\,\ln\left[\mathrm{Ce}_m(u,\lambda_m)\right]\right)_{u=u_0}} \quad \text{even} \tag{32}$$

$$\frac{\varepsilon_1(\omega_{mq})}{\varepsilon_2(\omega_{mq})} = \frac{\left((\partial/\partial u)\,\ln\left[\mathrm{Gek}_m(u,\lambda_m)\right]\right)_{u=u_0}}{\left((\partial/\partial u)\,\ln\left[\mathrm{Se}_m(u,\lambda_m)\right]\right)_{u=u_0}} \quad \text{odd}. \tag{33}$$

(34)

We follow the procedure of section 2 and display the interface mode dispersion by plotting the quantity $P$ (equation (6)). The variation of $P$ with the axial wavevector is depicted in figure 4. The density of interface modes is again highest near $P = 0$. It is noted that the degeneracy of the $m \neq 0$ interface modes of the circular wire is lifted by the asymmetry of the ellipse, in analogy to the splitting of the electronic subbands in figure 3.

Figure 5 shows the behaviour of the first-order interface mode potential for varying eccentricities. The striking behaviour that the potentials tend to localize near the region

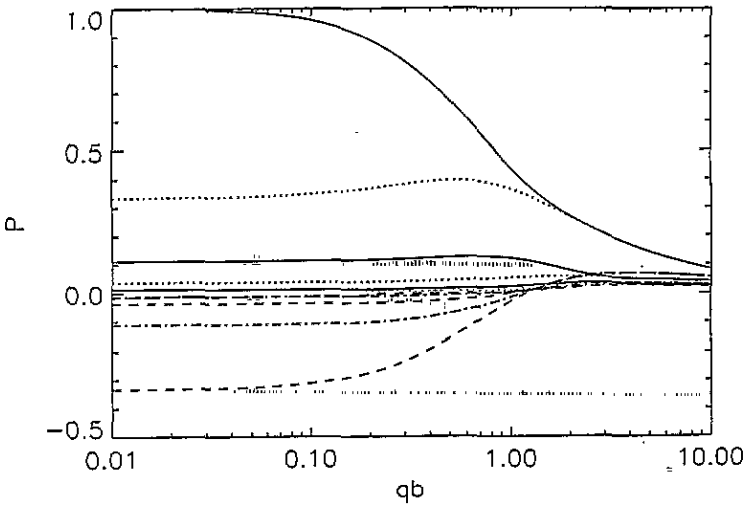


**Figure 4.** $P$ as a function of axial wavevector $qb$ for an ellipse with $a = 2b$. The curves are labelled in the same manner as figure 3 for the symmetry of the various modes shown.

of higher curvature is already apparent for an ellipse with $a = 2b$, and for $a = 10b$ this behaviour is even more apparent. This is in contrast to the trend for the electron wavefunction and the potential of the confined modes which tend to move away from the areas of higher curvature as $a$ increases. This difference in behaviour can be explained by considering the angular equation (20) as a Schrödinger equation [24] with 'potential' $2|\lambda|\cos(2v)$. This 'potential' is illustrated in figure 6 for an ellipse with $a = 2b$. The electrons and confined photons have $\lambda > 0$ and in the language of the analogous Schrödinger equation behave like 'electrons' and hence tend to be found at 'potential' minima which in this case means $\cos(2v) = -1$ (hence $v = \pi/2$ and $3\pi/2$) i.e. the region of minimum curvature (as shown in the diagram). The interface phonons, in contrast, have $\lambda$ negative, hence they are the analogues of holes, and therefore are to be found at 'potential' maxima, which corresponds to $\cos(2v) = 1$ (hence $v = 0$ and $\pi$) i.e. the regions of maximum curvature. In fact this maximum in the 'potential' occurs at the foci of the ellipse. Although we have concentrated here on the lowest-order modes, the analogy also holds for modes with higher quantum numbers. For these higher-order modes $\beta$ and $\lambda$ become more comparable and the modes can spread out from the lowest-curvature region (in the electron and confined phonon case) or the highest-curvature regions (for the interface modes). We therefore expect that for intrasubband scattering the higher-order interface modes will couple more efficiently to the ground state electrons compared with the coupling of the lowest-order interface mode as the eccentricity of the wire increases. This is due to their larger overlap with the electronic wavefunction at the centre of the ellipse.

## 5. The electron–phonon scattering rates

It is straightforward to quantize the potentials associated with the confined and interface modes of the elliptical wire following the methods employed in section 2 for the circular wire. The integrals involved cannot be case in closed analytical form in this case, and the expressions are as a consequence rather cumbersome. For this reason the details are not presented here. Once the phonons are quantized we can evaluate the scattering rate $W$

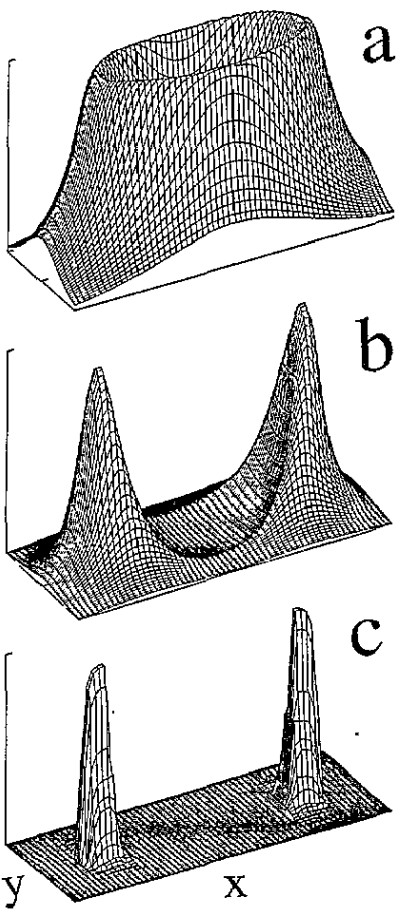


**Figure 5.** The elliptic interface mode potential for (a) $a = b$, (b) $a = 2b$ and (c) $a = 10b$.

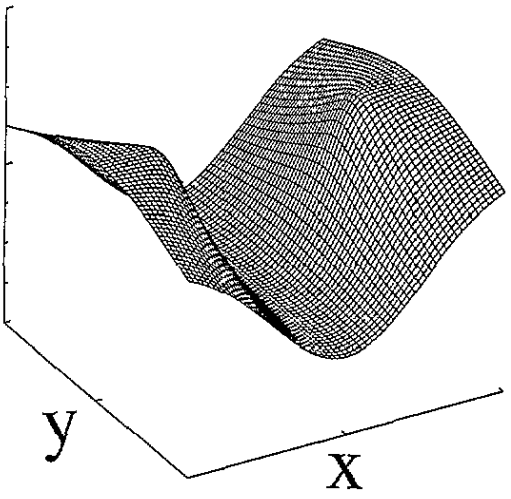


**Figure 6.** The effective angular 'potential' for an ellipse with $a = 2b$.

using Fermi's golden rule. In this section we, therefore, go beyond the work of Knipp and Reinecke [24] by coupling the optical phonons of an elliptical wire to the electrons.

Figure 7 displays the scattering rate as a function of the axial electron energy for an elliptical GaAs wire ($b = 50$ Å, $a = 2b$) embedded in AlAs (note that the area of this ellipse corresponds to a circular wire of radius 70.7 Å). The results illustrated in figure 7 are qualitatively similar to those predicted for a rectangular wire using a rather more sophisticated numerical procedure in order to correctly deal with the sharp corners [31].

In figure 8, we display the scattering rates versus $a/b$ for a fixed axial energy of 60 meV and $b = 50$ Å in the GaAs/AlAs structure. The total rate lies between that obtained by bulk GaAs and bulk AlAs phonons and confirms the sum rule for electron–phonon interaction [3, 6]. What is evident from this figure is the importance in the rates of the higher-order interface modes as the eccentricity of the elliptical wire increases accompanied by a corresponding decrease in the rates of lower-order modes. This is in accord with the 'potential' analogue of the previous section in which the higher-order interface modes are

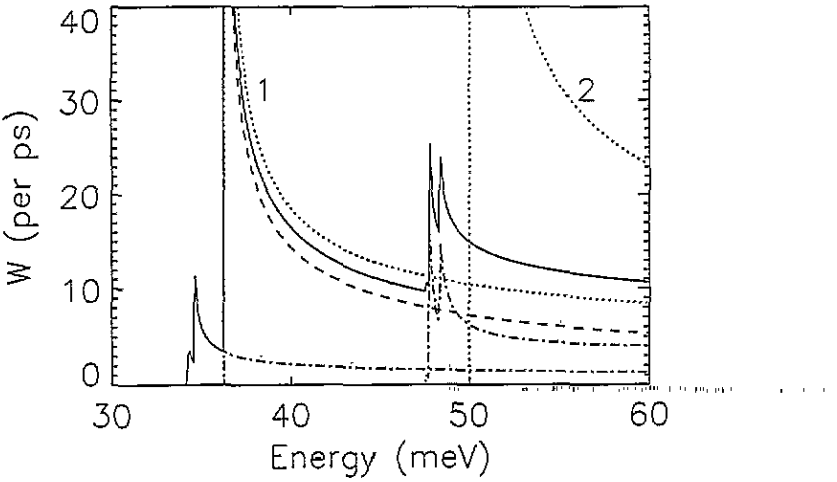


**Figure 7.** The scattering rate for an embedded elliptical wire for $b = 50$ Å and $a = 2b$. The solid curve corresponds to the total rate. The dashed curve is the rate due to the confined modes of the ellipse allowed via the selection rules. The dot–dashed curve that begins around 34 meV is the contribution from the GaAs interface modes which are allowed to contribute by the selection rules. The other dot–dashed curve corresponds to the contribution from the allowed AlAs interface modes. The dotted curve labelled 1 corresponds to scattering via bulk GaAs phonons and the dotted curve labelled 2 to that by bulk AlAs phonons.

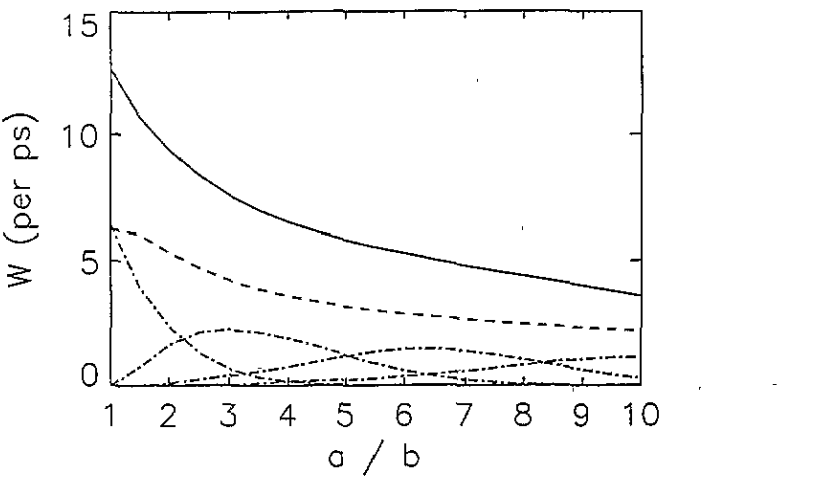


**Figure 8.** The scattering rate for a GaAs/AlAs elliptical quantum wire with $b = 50$ Å as a function of $a/b$ for fixed $E_k = 60$ meV. The solid curve is the total rate whilst the dashed curve is the contribution from the allowed confined GaAs modes. The dot–dashed curves represent the contribution from the allowed AlAs interface modes. It is noted that as $a/b$ increases the higher-order AlAs interface modes contribute more significantly. The contribution from the allowed GaAs interface modes is small and not depicted in the diagram for clarity although their contribution is included in the total rate.

known to overlap more strongly with the electronic states as the eccentricity of the wire increases.

Finally, as the eccentricity of the ellipse increases it is possible to go from the results

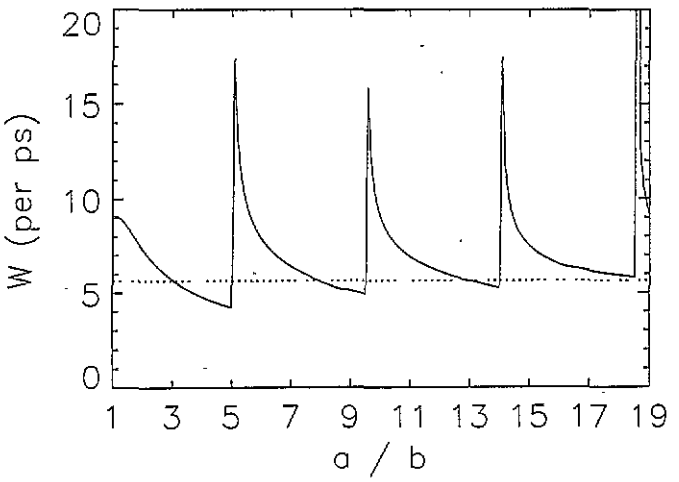


**Figure 9.** The total emission rate via confined modes as a function of $a/b$ ($b = 75$ Å) for an electron with an initial axial energy of 44 meV in the lowest subband. The dotted line is the 2D result.

of the cylinder to those of a slab. To obtain the intrasubband scattering rates of a quantum well, all possible intersubband and intrasubband transitions need to be taken into account and summed over. We illustrate this 1D to 2D transition for scattering via the emission of confined modes in figure 9. The electron is assumed to have a fixed axial energy of 44 meV within the lowest subband. As $a/b$ is increased ($b$ is fixed at 75 Å), infinities in the total rate occur whenever scattering into a new subband becomes permissible. These infinities are again due to the divergent nature of the 1D density of states, and the results are similar to those obtained by Bockelmann [28].

## 6. Conclusions

In this paper we have considered in detail the intrasubband scattering rates of embedded circular and elliptical GaAs quantum wires for electrons interacting with optical phonons calculated using the DC model. The choice of an elliptical geometry leads to analytically well behaved solutions of the Schrödinger and Laplace equations. Quantitative differences are exhibited between the cylindrical and the elliptical wires, in particular the non-trivial angular behaviour of the electrons and phonons which was shown to lead to an effective angular 'potential' that confines the lower-order electrons and confined phonons along the minor axis of the elliptical wire and the interface phonons to the regions of higher curvature, the 'corners' of the wire.

The assumption of an infinite confining potential for the electrons is of course only an approximation which, nevertheless, should give a reasonable estimate of the scattering rates and has been often employed for Q2D and Q1D calculations. Comparisons of the rates obtained via this approximation for a circular wire have been made [10, 13] with the conclusion that the intrasubband rates are reduced if a realistic finite potential is made. The inclusion of a finite confining potential in the case of an elliptical wire is much more complicated as compared to the circular case. This is due to the dependence of the angular electronic wavefunction functions on the wavevector on either side of the interface. The

reader is directed to the work of Nag and Gangopadhyay [32] for further details where a comparison of the subband energies in an elliptical wire using a infinite and a finite confining potential is made.

As has already been pointed out in the introduction, the DC model gives a good agreement for the *total* scattering rate in the GaAs/AlAs system compared with results emerging from microscopic calculations and from the more sophisticated hybrid model for the optical phonons [2, 33–38]. Despite its success in predicting the total scattering rate, the DC model suffers from shortcomings as regards Raman and micro-Raman measurements. It is therefore of considerable interest to investigate the behaviour of the more realistic hybrid phonons in such wires, as such a description is required in order to properly understand Raman measurements from such novel structures. The use of these more sophisticated continuum models which include bulk dispersion are crucial in a proper understanding of the observed Raman frequencies in the analogous Q2D systems [39]. It is anticipated that such Raman measurements will be carried out in the near future on quantum wires with cross-sectional areas small enough to observe confined phonon effects. Narrow free-standing wires [40] are possible candidates for such an investigation.

## Acknowledgments

We thank Dr N Postagioglu for useful discussions at the early stages of this work. CRB thanks the EPSRC for a studentship. This work is supported by the EPSRC under grant number GR/J80269.

## References

[1] Jaros M 1989 *Physics and Applications of Semiconductor Microstructures* (Oxford: Clarendon)
[2] Constantinou N C and Ridley B K 1994 *Phys. Rev.* B **49** 17 065
[3] Rucker H, Molinari E and Lugli P 1991 *Phys. Rev.* B **44** 3463; 1992 *Phys. Rev.* B **45** 6747
[4] Bhatt A R, Kim K W, Stroscio M A and Higman J M 1993 *Phys. Rev.* B **48** 14 671
[5] Wendler L 1985 *Phys. Status Solidi* b **129** 513
[6] Mori N and Ando T 1989 *Phys. Rev.* B **40** 6175
[7] Al-Dossary O, Babiker M and Constantinou N C 1992 *Semicond. Sci. Technol.* B **7** 91
[8] Tsen K T, Wald K R, Ruf T, Yu P Y and Morkoc H 1991 *Phys. Rev. Lett.* **67** 2557
[9] Ozturk E, Constantinou N C, Straw A, Balkan N, Ridley B K, Ritchie D A, Linfield E H, Churchill A C and Jones G A C 1994 *Semicond. Sci. Technol.* **9** 782
[10] Constantinou N C and Ridley B K 1989 *J. Phys.: Condens. Matter* **1** 2283
[11] Ahn D 1991 *J. Appl. Phys.* **69** 3596
[12] Campos V B and Das Sarma S 1992 *Phys. Rev.* B **45** 3898
[13] Leao S A, Hipolito O and Peeters F M 1993 *Superlatt. Microstruct.* **13** 37
[14] Shadrin V D, Kistenev F E and Serzhenco F L 1994 *J. Appl. Phys.* **75** 985
[15] Wang X F and Lei X L 1994 *Phys. Rev.* B **49** 4780
[16] Campos V B, Das Sarma S and Stroscio M A 1992 *Phys. Rev.* B **46** 3849
[17] Selbmann P E and Enderlein R 1992 *Superlatt. Microstruct.* **12** 219
[18] *Stroscio M A, Kim K W and Rudin S 1991 Superlatt. Microstruct.* **10** *55*
[19] Constantinou N C and Ridley B K 1990 *Phys. Rev.* B **41** 10 622, 10 627
[20] Rossi F, Bungaro C, Rota L, Lugli P and Molinari E 1994 *Solid State Electron.* **37** 761
[21] Adachi S 1985 *J. Appl. Phys.* **58** R1
[22] Ruppin R and Engleman R 1970 *Rep. Prog. Phys.* **33** 149
[23] Watt M, Sottomayor-Torres C M, Arnot H E G and Beaumont S P 1990 *Semicond. Sci. Technol.* **5** 285
[24] Knipp P A and Reinecke T L 1992 *Phys. Rev.* B **45** 9091
[25] Gold A and Ghazali A 1990 *Phys. Rev.* B **41** 7626
[26] Masale M and Constantinou N C 1993 *Phys. Rev.* B **48** 11 128
[27] Wendler L and Grigoryan V G 1994 *Phys. Status Solidi* b **181** 133

[28] Bockelmann U 1994 *Semicond. Sci. Technol.* **9** 865 and references therein
[29] McLachlan N W 1947 *Theory and Applications of Mathieu Functions* (Oxford: Clarendon)
Abramowitz M and Stegun I A 1970 *Handbook of Mathematical Functions* (New York: Dover)
[30] Bennett C R unpublished
[31] Knipp P A and Reinecke T L 1994 *Solid State Electron.* **37** 1105
[32] Nag B R and Gangopadhyay S 1993 *Phys. Status Solidi* a **179** 463
[33] Nash K J 1992 *Phys. Rev.* B **46** 7723
[34] Ridley B K 1993 *Phys. Rev.* B **47** 4592
[35] Constantinou N C, Al-Dossary O and Ridley B K 1993 *Solid State Commun.* **86** 191; 1993 *Solid State Commun.* **87** 1087
[36] Chamberlain M P, Cardona M and Ridley B K 1993 *Phys. Rev.* B **48** 14356
[37] Constantinou N C 1993 *Phonons in Semiconductor Nanostructures (NATO ASI Series E 236)* ed J P Leburton, J Pascual and C Sottomayor-Torres p 113
[38] Comas F, Trallero-Giner C and Cantarero A 1993 *Phys. Rev.* B **47** 7602
[39] Shields A J, Cardona M and Eberl K 1994 *Phys. Rev. Lett.* **72** 412
[40] Viswanath A K, Hiruma K and Katsuyama T 1993 *Superlatt. Microstruct.* **14** 105
Hiruma K, Yazawa M, Haraguchi K and Ogawa K 1993 *J. Appl. Phys.* **74** 3162